

# Automation of Visual Inspection of Photomasks for Microelectronic Products

T.S. Khodataeva<sup>1,A</sup>

Mari State University, Federal State Budgetary Educational Institution of Higher Education, Respublika Marii El, g.Ioshkar-Ola, Russian Federation

<sup>1</sup> ORCID: 0000-0002-6284-2292, [tkhodataeva@gmail.com](mailto:tkhodataeva@gmail.com)

## **Abstract**

The choice of a specific research topic was caused by a request for the development and implementation of automatic optical inspection at a semiconductor plant. The purpose of the work was to develop requirements, conduct technical design and create an optical control system for geometry deviations from a photomask drawing and a conductive pattern obtained using a manual stencil printer using relatively inexpensive equipment. As a result of the research, a pilot design sample of an automated optical control system using relatively inexpensive equipment was created and a computational algorithm was developed that ensures increased performance of the visual image recognition system, which allows to significantly reduce the percentage of defects. The work describes the implemented algorithm for obtaining images by an optical system and extracting images from a drawing file. Regardless of the method of obtaining an image (optical system, scanning electron microscope), there remains interest in choosing a criterion for comparing the obtained image with the reference one. The paper studies quantitative empirical metrics - Mean Square Error and Peak Signal-to-Noise Ratio for various noise reduction methods Block-Matching and 3D filtering and the classical spatial filtering method of Gaussian blur. The sensitivity of the structural similarity index metric to structural distortions of images after noise reduction is checked, taking into account the minimum values of the structural elements of metal-ceramic housings. Based on the Rosner test applied to the obtained values of the structural similarity metric, images containing defects are identified. The user interface provides for the output of the image area with a defect to the operator's screen.

**Keywords:** computer vision, visualization, image processing, drawing geometry, photomask, visual analysis, integrated circuit.

## **1. Introduction**

Due to the increased requirements for improving the quality of manufactured products of Semiconductor Devices Plant JSC (ZPP JSC), employees of the youth research laboratory "Development of Design and Technical Inspection of Printed Circuit Boards" of Mari State University were involved in identifying critical places in the production process and designing automatic optical control workplaces at the enterprise.

ZPP JSC has implemented a full technological cycle for the manufacture of more than 900 types of metal-ceramic cases (MCC) for integrated circuits (IC). Over the past five years, the technical level of parameters of IC cases manufactured using ceramic materials has grown significantly - the standard for designing the topology of cases is 80/80 microns, the diameter of the vias is from 80 microns, the number of holes in one case is up to 23,000.

At the moment, a simple visual inspection is used to control the quality of products at the enterprise. Personnel cannot cope with the task of quickly and accurately detecting defects.

Therefore, the priority area of product quality control is the technology of automatic optical inspection (AOI).

In the modern Russian market, AOI systems are represented exclusively by foreign suppliers: Viscom AG (Germany) [1], OMRON Corporation (Japan) [2] and many others. The embargo on the export of high-tech goods by the United States and the EU has led to high costs and problems with the purchase of products of this type.

The primary task of creating automatic optical control to identify defects arising from the manufacture of photomasks has been identified.

Preparation for the work was based on a large number of scientific works, both domestic and foreign authors, devoted to various aspects of the development of technological solutions for quality control of photomasks at different stages of their creation. Basically, the proposed methods used computer vision algorithms and implemented a variety of approaches for comparing defect patterns with images obtained in various ways.

The paper [3] proposes a methodology for checking and eliminating mask defects using both an image of mask defects obtained using a scanning electron microscope (SEM) and an image of optical control mask defects. Methods of modeling various processes were actively used in the work. Using digital processing algorithms, edges were extracted from the SEM images of the mask, converted into polygons, and mask defect patterns were formed. Templates were stored in the database. Such templates made it possible to make more accurate contour modeling. A simple optical model was used to obtain the simulated intensity of the photograph in the area surrounding the mask defect. Process sensitivity properties were extracted from the area surrounding the mask defect using a lithographic model. In total, templates were developed for 20 types of defects, including defects found in typical real-world circuit environments with 30 different sizes designed for each type.

Article [4] describes one of the main elements of the modular automated grid defect monitoring platform - the defect detection subsystem. For control, three types of mask images obtained in transmitted and reflected light, as well as a phase-contrast image, are used. Comparison models are constructed from optical images collected from a grid and generated from design data, where drawing elements are presented both as individual figures and as clusters of figures. In the proposed method, pixel-by-pixel comparison is replaced by comparison of parametric models of drawing elements. The method allows you to check with different accuracy.

Regardless of the method of obtaining the image, the choice of the criterion for comparing the obtained image with the reference one remains relevant.

The article is organized as follows. In Section 2, to identify critical points of product quality control, the technological process of production of the metal-ceramic housing is considered. Section 3 presents the configuration of the optical system, including hardware and software. Section 4 describes the algorithm for identifying defects arising from the manufacture of photomasks and presents the results of the study. The last section contains the corresponding conclusions.

## **2. Process Flow**

To identify critical points of quality control of products, it is necessary to study in detail the technological process of the production of MCC [5] (Fig. 1).

Alumina, quartz sand, manganese carbonate and chromium are mixed with water in drum mills in specified proportions, then the mixture is dehydrated in spray dryers. The resulting powder is sintered at a temperature of 1480-1500°C. At the same time, the powder components are combined with the transition of alumina into a stable alpha-form, which determines the structure of the ceramic material. The finest powders serve as the basis for the manufacture of ceramic tape. The ceramic tape is cut into strips of the desired width and into cards of a given size. Next, perforation takes place - punching holes with a tolerance of 100 microns

for the size of the holes, after which, using a manual stencil printer, a conductive pattern is applied to them with tungsten and molybdenum metallization pastes.

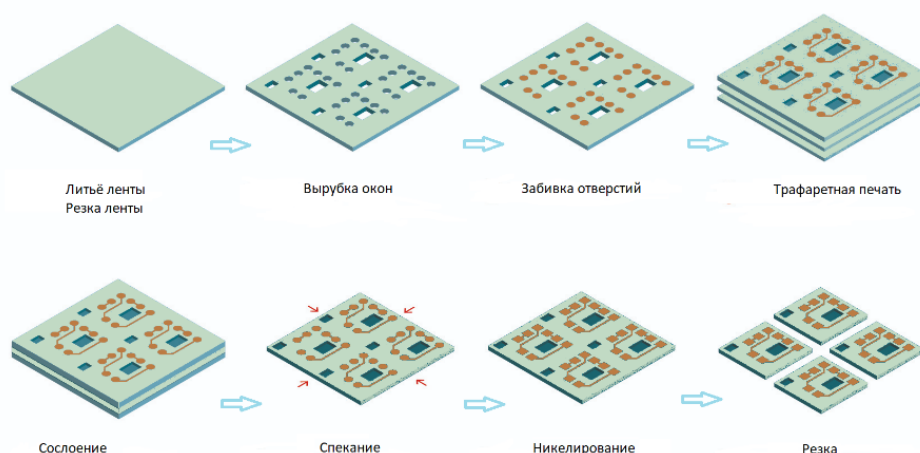


Fig. 1 Basic process for manufacturing metal-ceramic cases for integrated circuits

The quality of the ceramic substrate directly depends on the quality of the stencils. Practice has shown that the stencil can be changed about once every five working days after about 1,500 prints have been obtained from it.

The quality of the stencils is monitored by visual inspection of the printed pattern under a microscope. Visual inspection does not meet the requirements of modern production. The organization of automatic optical inspection at this stage will increase the productivity and efficiency of the inspection.

Ceramic substrates are assembled layer by layer into "packages" in accordance with the design documentation. The assembled bag on a special machine is packed in a shell, from which air is pumped out, after which the bag is placed in an isostatic press. Billets are fired in a nitrogen-hydrogen furnace. In this case, metal tracks are burned into the layers of ceramics. During the firing process, the boards are reduced in size.

The developments described in the following articles are of considerable interest for further studies of deformations during the roasting process of the MCC. Articles [6, 7] show the creation of a specialized machine vision platform and consider a number of issues of video recording of processes in isolated environments, determining the boundaries of objects in the image, analyzing and processing visual data, forming and presenting a picture of heat distribution in a three-dimensional object based on the results of a numerical experiment in accordance with the mathematical model of the process under study. The articles demonstrate the results of combining calculated data on the geometry of the product, the results of visual observation and thermal distribution data.

In the article [8], contactless optical methods for determining displacement and deformation fields on the surface of bodies are studied to assess deformations: correlation of digital images and electronic digital speckle interferometry, supplemented by elements of artificial intelligence, which makes it possible to build two-way connections between a real and a virtual object, which is not a finished product, but a technological process.

Such approaches will allow technologists to simplify the analysis of the production process, identify critical areas and select process parameters.

### 3. Optical system configuration

Based on foreign analogues, an experimental design model of an automated optical control system was designed, which required the creation of both hardware and software.

The hardware includes a lighting module, a servo-driven motion control unit based on a ball-screw pair based on an Arduino controller, an image acquisition module - a digital cam-

era, a microscope, a computer with software for processing images and detecting defects. To illuminate the scanned area, a complex backlight is used, consisting of an RGB-LED ring. To illuminate the scanned area, a complex backlight is used, consisting of an RGB-LED ring.

Open source Python packages were used to create the software. This is due to the simplicity of the syntax and interpretability on all popular platforms. References to the packages used will be given in Section 3.

A computer with the following characteristics was used as a test system:

- CPU: Intel® Core™ i7-10700, 2.90GHz.
- RAM: 32Gb.
- OS: Windows 10 Pro.

## 4. Description of the defect detection algorithm

The photomask is a plane-parallel transparent plate with an opaque coating, usually a thin layer of chromium. The material of the photomask was mainly quartz glass. Defects arising in the manufacture of photomasks are associated with the technology of lithographic processes used for their manufacture - these are impurities, scratches, loss of adhesion, excess masking material (influx, edge protrusion), defect of edge rust.

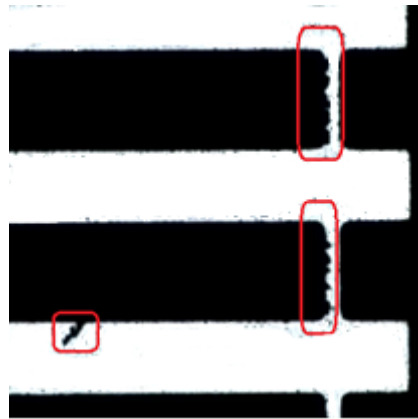


Fig. 2. Example of photomask defects: edge protrusion and edge rub defect

Any deviations of the geometric dimensions of the product from the drawing that arose during the manufacture of the photomask are perceived as defects.

To create architectural drawings of metal-ceramic housing templates, specialized CAD systems (Computer-Added Design systems) are used: AutoCAD [10], Altium Designer [11] and others. The drawing data of the photomask is contained in a binary dwg file (from the English drawing - drawing) [12], which is the main format for storing two-dimensional (2D) and three-dimensional (3D) design data and metadata. This format is the AutoCAD storage standard. In CAD systems, the topology of a designed MCC is the intersection and overlay of layers. For this topology, conversion to the dxf format is implemented - a universal drawing exchange format. Dxf files are standard ASCII text files that contain vector-based information. Vector data representation provides high image accuracy when scaled.

To control deviations of the photomask geometry from the drawing:

Extract data from a photomask drawing. Scale the drawing data in vector representation and convert it to raster form.

Obtain enlarged raster images of the photomask using an optical system.

Select the noise reduction algorithm for the images acquired by the optical system.

Propose and test the criterion for comparing the obtained image with the reference one, which is the drawing.

For analysis, there are enlarged fragments of the (raster) image of the photomask obtained by the optical system, as well as the MCC drawing in dwg format, which is converted into a vector representation in the form of a dxf file.

For comparison, you need to bring the images to a single raster view. To work with drawing data: converting formats, extracting layers, scaling, splitting into fragments and saving in raster form, the libraries ezdxf [13]13, odfc [14] were used.

The figure shows an example of a drawing of a 40mm x 40mm MCC photomask (Fig. 3.).

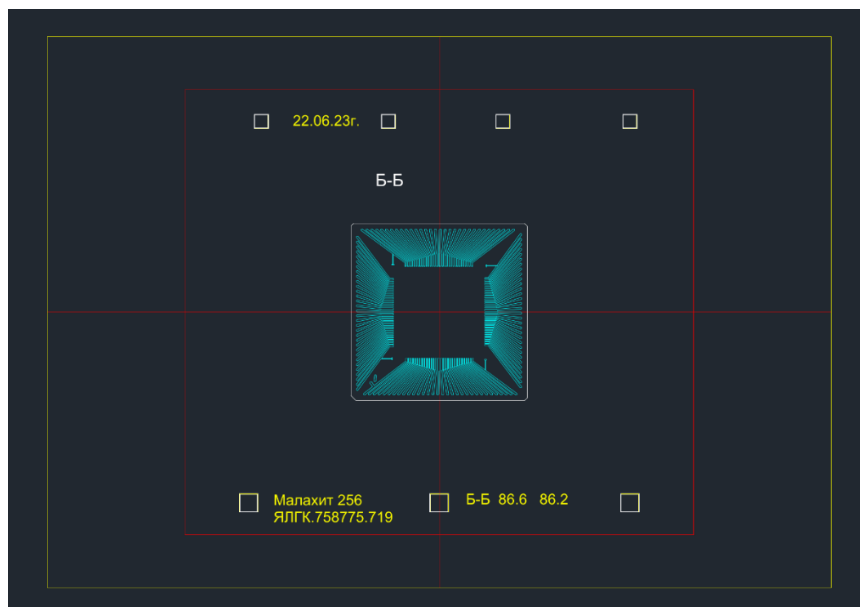


Fig. 3. Full AutoCAD Photo Template Drawing

For comparison with images obtained by the optical system, a layer with reference points and a layer containing an image of the FCS are selected from the drawing file. Then an additional dxf file is created, combining only the selected layers (Fig. 4.).

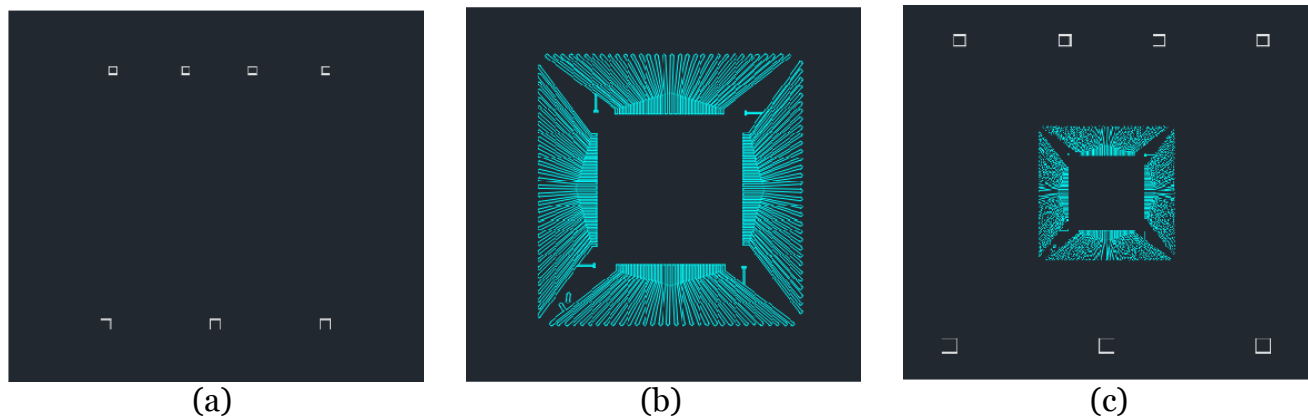


Fig. 4. a, b are layers extracted from the dxf file, c are layers merged and saved to an additional dxf file

In the program, the additional dxf file is divided into segments in accordance with the number of images received from the camera, scaled to the corresponding size of images received from the camera, and saved in raster form (Fig. 5.).

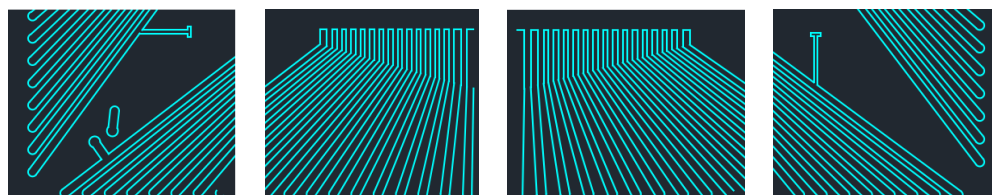


Fig. 5. Saved Drawing Dxf File Segments

To control the movement of the optical system and calculate the size of images taken from the camera, you need to know the field of view and resolution of the digital camera, the magnification of the microscope. Then you can use the formulas:

$$F \approx \frac{L}{ab}$$

$$F_{px} = \frac{P}{ab}$$

where  $F$  is the field of view in mm,  $L$  is the matrix size in mm,  $a$  is the lens magnification factor,  $b$  is the adapter magnification factor,  $P$  is the camera pixel size in  $\mu\text{m}$ ,  $F_{px}$  is the resolution in  $\mu\text{m}/\text{pixel}$ . All necessary values are extracted from the technical documentation containing the characteristics of the products used.

To obtain images, a ToupCam U3CMOS14000KPA digital camera was used: sensor size 5.73x4.6 mm, pixel size 1.4x1.4  $\mu\text{m}$ , with a C-mount adapter of 0.5x; and a 3x magnification microscope lens. The field of view of the resulting image of the photomask was 3.82x3.09mm. One pixel corresponds to an object of 0.9  $\mu\text{m}$ . The size of the entire photo template is extracted from the dxf file.

The presence of noise in the images is due to the design feature of the digital camera and the photonic nature of the light. To ensure the required level of quality of the analysis, it is important to choose the correct noise reduction algorithm without losing image features. The main criteria in this case are the contours of the image that should not be blurred, as well as small details of the image that should not be destroyed along with the noise component.

The classic image comparison process is based on noise modeling: a good quality image is taken, noise is added (Fig. 6.). Then the image restored from noise by various methods is considered. Many noises can be approximated quite well by the additive Gaussian noise model. The open source packages OpenCV (Computer Vision Library) [15] and bm3d [16] were used for experiments.

Quantitative empirical metrics are used to compare image enhancement algorithms, in particular,  $MSE$  (Mean Square Error) and  $PSNR$  (Peak Signal-to-Noise Ratio) [17].

The  $MSE$  is the mean of the squares of "errors" between the real and reconstructed images. The peak signal to noise ratio ( $PSNR$ ) is an expression for the ratio between the maximum possible signal value (power) and the power of distorting noise affecting the quality of its presentation.

The image is a two-dimensional array of grayscale data. The mathematical representation of  $MSE$  and  $PSNR$  is as follows:

$$MSE = \left(\frac{1}{NM}\right) \sum_{n=1}^N \sum_{m=1}^M |x(m, n) - y(m, n)|^2$$

where  $x, y$  are areas inside the sliding window for images;  $N, M$  - sliding window dimensions;  $m, n$  is the column and row number of the image pixel.

$$PSNR = 10 \log_{10} \frac{MAX_I^2}{MSE} \quad (1)$$

where  $MAX_I$  is the maximum value received by the image pixel. For pixel bitrates of 8 bits,  $MAX_I = 255$ .

According to expression (1), if one or another image processing method works better, the  $PSNR$  measure will take a larger value, since in this case the reference and processed images will be quite close. For the  $MSE$  metric, the opposite is true - the lower the  $MSE$  value, the higher the similarity.

The paper studied the results of noise reduction of the classical method of spatial filtering of Gaussian blur [18] and one of the most effective and popular noise reduction methods in recent years - BM3D (Block-Matching and 3D filtering) [19]. BM3D is a two-step non-local co-filtering method in the transform domain. In this method, similar patches (images of a small area of  $3 \times 3$  or  $5 \times 5$  pixels) are combined into 3D groups by matching blocks, and 3D groups are converted to a wavelet domain. Rigid thresholding is then applied in the wavelet



region. Finally, after inverse coefficient transformation, all estimated areas are combined to reconstruct the entire image.

Noise reduction methods based on convolutional neural networks DnCNN [20], FFDNet [21], Noise2Void (CNN) [22] were not considered, since professional optics were used to obtain images: a high-resolution camera, sufficient illumination and static.

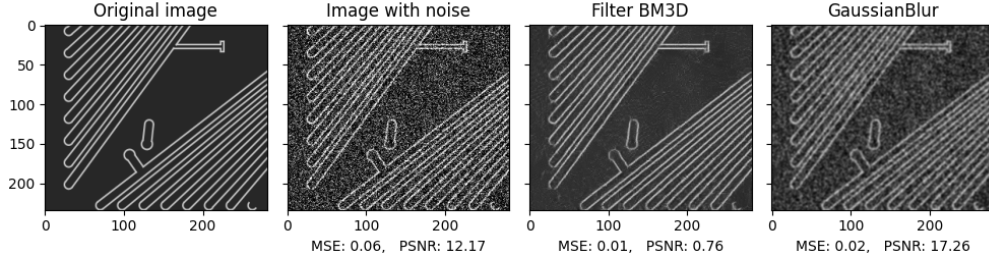


Fig. 6. Noise modelling to calculate metrics

The table (see Table 1) shows the average PSNR and MSE results obtained by processing 460 images with different levels of simulated Gaussian noise.

TABLE 1 AVERAGED PSNR & MSE

	<b>GaussianBlur</b>		<b>BM3D</b>	
6	MSE	PSNR	MSE	PSNR
0,01	0.0013	28.97	0.0011	30.32
0,1	0.0077	21.16	0.0050	23.09

Although the Gaussian blur method was superior to the BM3D method in terms of speed, we opted for BM3D, since the topology tolerances on the map are less than 10 microns.

The images obtained by the optical system are converted to shades of gray and cleared of noise by the BM3D method. The main defects in the geometry of the photomask occur on the contours of topological elements. To obtain more pronounced contours, the contour amplification method was used using the Sobel operator [23], by adding an image to an image obtained using the Sobel operator from the scikit-image library [[24]. The Sobel operator is based on convolution of the image with small integer filters in the vertical and horizontal directions, so it is relatively easy to calculate. The operator uses kernels  $3 \times 3$ , with which the original image is folded to calculate the approximate values of the derivatives horizontally and vertically.

Images are binarized using the Otsu method [25] of optimal global threshold transformation. In this method, the threshold values are automatically selected according to the histogram of the distribution of intensity values of the original image.

The *MSE* and *PSNR* metrics do not perform well in recognizing structural content in images, therefore, at the stage of finding defects, the *SSIM* (Structural Similarity Index Measure) was chosen to assess the differences in images [26] as an indicator of the structural similarity index.

The local SSIM index measures the similarity of three image patch elements: the similarity of  $l(x, y)$  local brightnesses (brightness values), the similarity of  $c(x, y)$  local patch contrasts, and the similarity of  $s(x, y)$  local patch structures. The index is based on local SSIM scores between two  $x$  and  $y$  windows of size  $N \times N$  pixels calculated around the corresponding pixels in images A and B, according to the formula:

$$SIMM(x, y) = \frac{(2 \mu_x \mu_y + c_1)(2 \sigma_{xy} + c_2)}{(\mu_x^2 + \mu_y^2 + c_1)(\sigma_x^2 + \sigma_y^2 + c_2)}$$

where  $\mu_x$  is the average pixel sample value in the  $x$  window;  $\mu_y$  - average value of pixel sampling in the  $y$  window;  $\sigma_x^2$  - variance in window  $x$ ;  $\sigma_y^2$  - variance in the window  $y$ ;  $\sigma_{xy}$  - covariance of windows  $x$  and  $y$ ;  $c_1 = (k_1 L)^2$  and  $c_2 = (k_2 L)^2$ ,  $L = 255$ , determining a dynamic brightness range;  $k_1 = 0.01$ ,  $k_2 = 0.03$  are experimentally determined constants.

The global SSIM index for images A and B is calculated as the arithmetic mean of the local scores using the formula:

$$SIMM(A, B) = \frac{1}{M} \sum_{x,y} (SSIM(x, y))$$

It was necessary to test the sensitivity of the structural similarity index metric to structural distortions of images after noise reduction. For this purpose, the resulting set of segmented images of a particular MCC dxf file (these are ideal images) were noisy using an additive Gaussian noise model. Between the ideal and noisy images, the  $SSIM_i$  metric was calculated, and then the  $SSIM_r$  metric was calculated between the ideal images and the images of the photomask obtained using the optical system. The images of the photomask obtained for the experimenters using the optical system had defects. These calculations were followed by the application of the Rosner emission test [27] implemented in the PyAstronomy.pyasl.generalizedESD library [28] on the  $R$  [ $R_i$ ] set, where  $R_i = abs(SSIM_i - SSIM_r)$ , (see Table 2, Fig. 7.). The Rosner test allows you to test several possible emissions and avoid the masking problem, in which the presence of several emissions masks the fact that at least one emission is present. The most extreme  $R_i$  values of the set  $R$  [ $R_i$ ] are outliers. This experiment allowed us to check the sensitivity of the structural similarity index metric to structural distortions of images after noise reduction, taking into account the minimum values of the structural elements of metal-ceramic housings.

The same approach is used to identify images with defects. In this case, it is sufficient to apply the Rosner outlier test only to the  $SSIM_r$  metric. The user interface displays the defective image area on the operator's screen. The user interface for displaying comparison results is implemented by the author based on the Qt library [29]29.

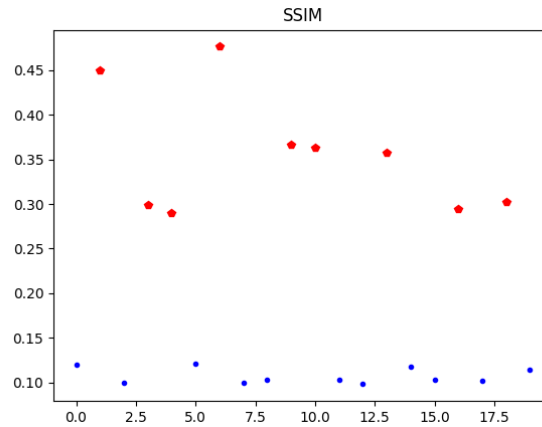


Fig. 7. Graphical representation of outliers for a set  $abs(SSIM_i - SSIM_r)$

TABLE 2 SSIM METRIC VALUE FOR PERFECT AND REAL IMAGES

	<b>SSIM<sub>i</sub></b>	<b>SSIM<sub>r</sub></b>	<b>abs(SSIM<sub>i</sub> - SSIM<sub>r</sub>)</b>
img_00	0.63233	0.51272	0.11961
img_01	0.96576	0.51594	0.44981
...	...	...	...
img_42	0.96843	0.66646	0.30197
img_43	0.61394	0.49945	0.11449

The work tested the method of identifying defects arising in the manufacture of photomasks. The SSIM structural similarity metric is used to compare the image template drawing divided into segments and images obtained by the optical system. Applying the Rosner emissions test to the metric of structural similarity between the reference images and the images obtained by the optical system allows the fragments of the photomask having the defect to be determined.



The software is written in Python. The open source ezdxf library was actively used to work with the photomask drawing file. The modules of this library made it possible to convert the source file to dxf-format, extract the drawing layers required for comparison, combine these layers for further work, scale the resulting vector image without distortion to the required size, split it into fragments, convert image fragments to a raster view and save as reference.

Using noise modeling based on quantitative empirical metrics MSE and PSNR, a BM3D noise reduction algorithm was selected. To enhance the contour of the image after noise reduction, the Sobel operator was used, and the Otsu method was used to binarize images.

The sensitivity of the structural similarity index metric to structural distortion of images after noise cancellation was tested.

The developed software and hardware complex allows you to carry out the entire cycle of work on the automated search for defects in photomasks.

## 5. Conclusion

The use of enclosures based on ceramic materials is necessary in cases where high requirements are imposed on the element base in terms of reliability and performance. The main areas of their application are space technology, military products, and other products operated in extreme conditions. At the same time, the manufacturing technology of such cases is quite complicated, which necessitates strict control of the quality of their manufacture. The closer the manufactured sample to the standard (stencil), the higher its quality. Thus, quality control is largely associated with the procedure for comparing manufactured cases (more precisely, their images) with given stencils.

Various AOI systems used in microelectronics make extensive use of image subtraction comparison to detect pixel-by-pixel differences. This method with various modifications is presented in many works, for example, in works [30, 31]31. In order for the pixel-by-pixel comparison to become practical, it is necessary to set a reasonable tolerance for it when performing the subtraction process. Such a criterion is quite subjective and does not meet the high requirements for reliability and accuracy of manufacturing the MCC.

This paper investigated quantitative empirical metrics. The sensitivity of the SSIM metric to structural distortions of images after noise reduction was tested, taking into account the minimum values of the structural elements of metal-ceramic cases, which are manufactured at modern serial production and are characterized by element size less than 40 microns. Obviously, the necessary quality control with an increasing volume of production cannot be implemented only by visual inspection of the printed pattern under a microscope. To improve the quality of control, a development model of automatic optical control was created.

The quality of the MCC directly depends on the quality of the photomasks. Practice has shown that you can change the stencil about once every five working days after about 1,500 prints are obtained from it. The frequency of checks depends on the complexity of the topological pattern: the most saturated ones are checked after each application, the simpler ones - after 5-10 cycles.

The described methodology was tested on several samples of photomasks for ceramic-metal cases. The methods and algorithms proposed in this work, which make it possible to identify defects at the early stages of the technological process, reduce the workload on personnel and significantly improve the quality of visual control, were implemented by the author in the form of software tools.

The development of the project will be associated with the development of a classification of defects and methods for localizing the area where the defect is found on the image. For this purpose, it is planned to use a neural network with the YOLO architecture [32]32. Currently, the formation of a set of image data containing various defects of photomasks has already begun, the first results on the classification of defects and marking of images for training a neural network have been obtained.

## Acknowledgements

The work is carried out within the framework of the state assignment for the provision of public services (performance of work) No. 075-01252-22-03 dated 26.10.2022.

## References

1. URL: <https://www.viscom.com> (accessed 2.08.2024)
2. URL: <https://www.ia.omron.com> (accessed 2.08.2024)
3. Simulation based mask defect repair verification and disposition / E. Guo, Sh. Zhao, S. Zhang [et al.] // Photomask Technology, Monterey, CA, United States. – 2009. – Vol. 7488. – Monterey, CA, United States, 2009. – P. 74880G-10. – DOI 10.1117/12.829692
4. Avakaw, S. High productivity object-oriented defect detection algorithms for the new modular die-to-database reticle inspection platform / S. Avakaw // Proceedings of SPIE - The International Society for Optical Engineering, Dresden/ editors: Behringer U.F.W., UBC Microelectronics, Germany. – Dresden. – 2005. – P. 290-299. – DOI 10.1117/12.637300.
5. Technological equipment and materials used for metal-ceramic package manufacture / Shugaepov S.H., Ermolaev E., Egoshin V., Akhmetgaliev R., Mazurenko // Electronics: Science, Technology, Business. – 2022. – № 5(216). – C. 62-65. – DOI 10.22184/1992-4178.2022.216.5.62.65.
6. Molotkov A.A., Tretiyakova, O.N. On possible approaches to visualizing the process of selective laser melting. Scientific Visualization. – 2019 – Vol. 11, No. 4. C. 1 – 12. – DOI 10.26583/sv.11.4.01
7. Molotkov A.A., Tretiyakova O.N., Tuzhilin D. N. About Development and Application of a Software Platform for Machine Vision for Various Laser Technologies. Scientific Visualization. – 2022 – Vol. 14, No. 5. C. 108 – 118. – DOI 10.26583/sv.14.5.08
8. Petrov M.A., Romashov D.A., Isakov V.V. Estimation of Sheet Deformation of Aluminium Blank using Non-Contact Methods on the Example of Erichsen Cupping Test. Scientific Visualization. – 2023 – Vol. 15, No. 4. C. 124 – 139. – DOI 10.26583/sv.15.4.10
9. Lavrova L.K., Electronic teaching aid in the discipline "Technology and equipment of lithographic processes" for the specialty 2-41 01 31 « Microelectronics » – 2019. 103 c.
10. URL: <https://www.autodesk.com> (accessed 2.08.2024)
11. URL: <https://www.altium.com> (accessed 2.08.2024)
12. DWG. URL: <https://ru.wikipedia.org/wiki/DWG> (accessed 2.08.2024)
13. A Python package to create/manipulate DXF drawings. – URL: <https://pypi.org/project/ezdxf> (accessed 2.08.2024)
14. ODA DWG-DXF Converter. – URL: [https://www.opendesign.com/guestfiles/oda\\_file\\_converter](https://www.opendesign.com/guestfiles/oda_file_converter) (accessed 2.08.2024)
15. Bradski G. The openCV Library. Dr Dobb's Journal: Software Tools for the Professional. – 2000. – URL: <https://opencv.org> (accessed 2.08.2024)
16. BM3D for correlated noise. URL: <https://pypi.org/project/bm3d> (accessed 2.08.2024)
17. Gonsales R., Woods R. Digital image processing 3-e Edition. Moscow, Technosphaera. – 2012. – C. 415-416. – ISBN 978-5-94836-331-8.
18. Tomasi C., Manduchi R. Bilateral filtering for gray and color images. //Sixth International Conference on Computer Vision IEEE: Bombay, India. – 1998. – P. 839–846. – DOI 10.1109/ICCV.1998.710815.
19. Dabov, K. Image Denoising by Sparse 3-D Transform-Domain Collaborative Filtering / Dabov, K. Foi, A., Katkovnik, V., Egiazarian, K. //IEEE Transactions on Image Processing. – 2007. – Vol. 16, No. 8. – P. 2080–2095. – DOI 10.1109/ TIP.2007.901238.
20. Zhang K. Beyond a Gaussian denoiser: residual learning of deep CNN for image denoising / Zhang K., Zuo W., Chen Y., Meng D., Zhang L. // IEEE Transactions on Image Processing. – 2017. – Vol. 26, No. 7, P. 3142–3155. – DOI 10.1109/TIP.2017.2662206.

21. Zhang K., Zuo L., Zhang W. FFDNet: Toward a fast and flexible solution for CNN-Based image denoising // IEEE Transactions on Image Processing. – 2018. – Vol. 27, No. 9. – P. 4608-4622. – DOI 10.1109/TIP.2018.2839891.
22. Krull A., Buchholz T., Jug F. Noise2void-Learning denoising from single noisy images // Proceedings of the IEEE Computer Society Conference on Computer Vision and Pattern Recognition: 32, Long Beach, CA. – Long Beach, CA. – 2019. – P. 2124-2132. – DOI 10.1109/CVPR.2019.00223.
23. Sobel, I. An Isotropic  $3 \times 3$  Image Gradient Operator. In Presentation at Stanford A.I. Project 1968; Academic Press: Cambridge, MA, USA, 2014. – DOI 10.13140/RG.2.1.1912.4965.
24. Van der Walt, S., Schönberger, J. L., Nunez-Iglesias, J., Boulogne, F., Warner, J. D., Yager, N., ... Yu, T. – 2014. scikit-image: image processing in Python. – 2014 PeerJ, 2, e453. DOI 10.7717/peerj.453. URL: <https://scikit-image.org> (2.08.2024)
25. Otsu N. A Threshold Selection Method from Gray-Level Histograms // IEEE Transactions on systems, MAN, and CYBERNETICS. – 1979 – Vol. SMC-9, No. 1. – P. 62-66.
26. Wang Z., Bovik A., Sheikh H. Simoncelli E, Image quality assessment: from error visibility to structural similarity // IEEE Transactions on Image Processing. – 2004. – Vol. 13, No. 4. – P. 600–612. – DOI 10.1109/TIP.2003.819861.
27. Rosner B. Percentage Points for a Generalized ESD Many-Outlier Procedure // Technometrics. – 1983. – Vol. 25, No. 2. – P. 165–172. – DOI 10.1080/00401706.1983.10487848.
28. IDL Astronomy User's Library.  
URLs: <https://pyastronomy.readthedocs.io/en/latest/pyaslDoc/aslDoc/outlier.html>,  
<https://pyastronomy.readthedocs.io/en/latest/pyaslDoc/aslDoc/outlier.html> (accessed 2.08.2024)
29. Qt Framework. URL: <https://www.qt.io> (2.08.2024)
30. Kaur B., Kaur G., Kaur A. Detection and classification of Printed circuit board defects using image subtraction method. // Recent Advances in Engineering and Computational Sciences, March 2014, DOI 10.1109/raecs.2014.6799537.
31. Pal A., Chauhan S., and Bhardwaj S. Detection of Bare PCB Defects by Image Subtraction Method using Machine Vision. // Proceedings of the World Congress on Engineering. – 2019 – Vol. 2.No. 11. P. 879-892.
32. Redmon J., Farhadi A. YOLO9000: Better, Faster, Stronger. IEEE Conference on Computer Vision and Pattern Recognition. – 2017. – DOI 10.48550/arXiv.1612.08242